Chapter 4
Learning the Temperature Dynamics During Thermal Laser Ablation

Given the research problem outlined in the previous chapter, here we focus on the development of a methodology to learn the temperature dynamics of tissues subject to thermal laser ablation. Chapter 2 introduced the equations that govern the generation of heat within the tissue during laser irradiation, and the associated increase of temperature. Such relations constitute the starting point of our investigation: based on these, we hypothesize that the superficial temperature of tissue can be modeled, at any given instant in time, as the superposition of Gaussian functions. Nonlinear fitting methods [1] are used to calculate the Gaussian parameters (amplitude, mean and variance) that describe the distribution of temperature at discrete moments in time. The learning problem is formulated as a supervised nonlinear regression, which aims to predict the temporal evolution of the Gaussian parameters.

To understand the viability of the proposed approach we first consider a simple scenario, which does not involve motions of the laser beam. Later in the chapter we present an extension of this methodology to a more general case, to estimate the temperature dynamics produced by a scanning beam.

4.1 Preliminary Considerations

The hypothesis function f defined in Eq. 3.1 estimates the superficial temperature of a slab of tissue subject to laser irradiation, given the applied laser power P, the pulse duration τ, the beam scanning frequency ω_s, and the total laser exposure time t_{exp}. Initial exploration was conducted to better understand the nature of function f and identify an appropriate set of basis functions for the learning task.

Let us consider a simple scenario in which a laser beam, TEM_{00} profile, irradiates a fixed spot on the surface R of a sample of tissue. This scenario is represented in Fig. 4.1. For the sake of simplicity, we assume that the surface of tissue is plain and that the laser beam is normally incident on it. We further assume that the laser is

L. Fichera, *Cognitive Supervision for Robot-Assisted Minimally Invasive Laser Surgery*, Springer Theses, DOI 10.1007/978-3-319-30330-7_4

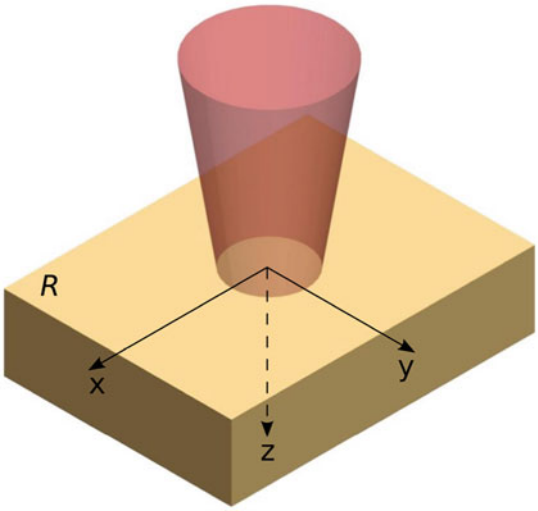

Fig. 4.1 Geometry of tissue irradiation

perfectly focused on the surface of tissue. A Cartesian reference frame (x, y, z) is established to describe the tissue geometry, with z being coincident with the beam axis, x and y laying on the R plane. Based on the heat conduction equation (Eq. 2.12), a local variation of tissue temperature occurs, that is modeled as the sum of two distinct contributions: the laser input S ($\mathrm{W} \cdot \mathrm{m}^{-3}$), plus a second-order differential term that accounts for the diffusion of heat within the tissue volume. Although a general formulation for the temporal evolution of temperature $T(t)$ cannot be given analytically, exact solutions can be derived under certain assumptions.

The "1 µs rule" (see Sect. 2.4.2) establishes that the effect of heat diffusion is negligible for short irradiations, i.e. for values of exposure time $t_{exp} < 1\mu\mathrm{s}$ [2]. In this case, the local temperature increase produced by the laser source is:

$$\dot{T} = \frac{1}{\rho c} S. \tag{4.1}$$

Let us recall from Chap. 2 that ρ is the density of tissue ($\mathrm{kg} \cdot \mathrm{m}^{-3}$) and c is its specific heat capacity ($\mathrm{J} \cdot \mathrm{kg}^{-1}\mathrm{K}^{-1}$). Replacing the volumetric energy density S with its definition (Eq. 2.7) yields

$$\dot{T} = \frac{\mu_a}{\rho c} I, \tag{4.2}$$

where μ_a is the absorption coefficient of tissue (m^{-1}). This equation establishes a relation between the temporal derivative of the temperature and the intensity profile I of the laser beam within the tissue volume. Such relation depends on the local values of the absorption coefficient μ_a, tissue density ρ and heat capacity c. Assuming that these coefficients are *isotropic*, i.e. that they are uniform across the tissue sample, it follows that the temperature increase produced by the laser has precisely the same

form of the beam intensity, i.e. a Gaussian function. The time dependency of I can be dropped if a constant beam intensity is used. In such a case, Eq. 4.2 has a straightforward solution:

$$T(x, y, z, t) = T_0 + \frac{\mu_a}{\rho c} I(x, y, z)\, t. \tag{4.3}$$

where T_0 is the initial temperature. Imposing $z = 0$ and replacing the intensity I by its definition (Eq. 2.5) we obtain a relation that describe the temporal evolution of the temperature on the surface of tissue:

$$T(x, y, t) = T_0 + \frac{\mu_a}{\rho c} I_0 \exp\left(-\frac{2(x^2 + y^2)}{\omega^2}\right) t. \tag{4.4}$$

We now consider the homogeneous part of the heat conduction equation, that models the temperature variation once the laser source is turned off (i.e. $S = 0$)

$$\dot{T} = \kappa \Delta T, \tag{4.5}$$

where κ is the temperature conductivity of tissue ($m^2 \cdot s^{-1}$). This equation admits solutions of the form[1]

$$T(x, y, z, t) = T_0 + \frac{\alpha \exp\left(-\frac{x^2+y^2+z^2}{4\kappa t}\right)}{(4\pi\kappa t)^{\frac{3}{2}}}, \tag{4.6}$$

with α being an integration constant. From this relation, it follows that the time-dependent distribution of temperature at the tissue surface follows a two-dimensional Gaussian profile:

$$T(x, y, t) = T_0 + \frac{\alpha \exp\left(-\frac{x^2+y^2}{4\kappa t}\right)}{(4\pi\kappa t)^{\frac{3}{2}}}. \tag{4.7}$$

These theoretical results seem to indicate that a combination of Gaussian functions could adequately approximate the superficial temperature of tissue during laser ablation. Nonetheless, in our derivation of Eqs. 4.4 and 4.7, we have used many assumptions that certainly do not hold in the case of laser ablation. The ablation process induces disruptive modifications in the tissue both at the mechanical and physical levels (alterations in the density, absorption and thermal conductivity), whereas the calculations above assume a fixed tissue geometry and isotropic conditions. Furthermore, the CO_2 lasers used in clinical practice present pulse durations $\tau \geq 1\mu s$: for these durations the effects of heat diffusion can no longer be neglected and, as it was pointed out earlier, the solution $T(t)$ must be extracted using numerical approximation methods. Based on these considerations, it is unclear whether a

[1] A proof is given in Appendix B.

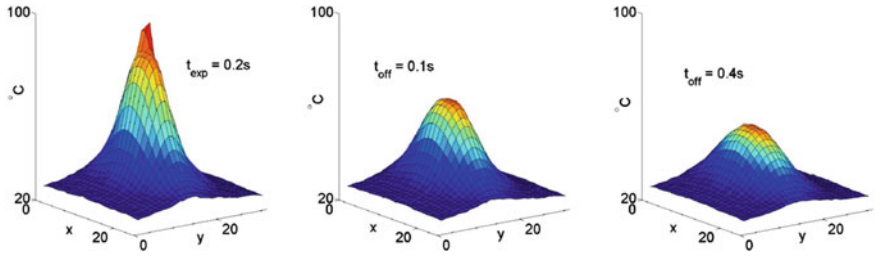

Fig. 4.2 Temperature distribution captured at different moments of the experiment. **a** Laser exposed for $t_{exp} = 0.2\,\text{s}$, **b** After exposure, laser is turned off ($t_{off} = 0.1\,\text{s}$) and **c** $t_{off} = 0.4\,\text{s}$. Reproduced from [3] with kind permission from Springer Science+Business Media

Gaussian model is adequate for the approximation of the superficial tissue temperature T. To better understand the validity of this hypothesis, we performed a series of preliminary laser experiments.

Agar-based gel phantoms were irradiated with a CO_2 laser source (beam waist $\omega_s = 250\,\mu\text{m}$), using an exposure time $t_{exp} = 0.2\,\text{s}$. The superficial temperature was captured with an infrared thermal camera, at a rate of 100 Hz. This sensor provides a sequence of images that contains the values of temperature for a predefined continuous rectangular plane S centered at the point of laser incision. Before being irradiated, the samples were kept at room temperature ($\sim$25 °C) for 10 min. The sequence in Fig. 4.2 shows typical temperature profiles obtained during the trials: the xy plane of the plot corresponds to the surface of the tissue, values of temperature have been plotted in the z-axis. Each pixel represents the temperature value (°C) of an area that covers $0.177 \times 0.177\,\text{mm}^2$.

Visual analysis of the plots in Fig. 4.2 indicates that the superficial temperature of tissue can be reasonably assumed to have a Gaussian distribution. Temperature spikes are observed during laser irradiation, next to the peak of the Gaussian surface. These might be produced by the expulsion of hot plume from the ablation site.

4.2 Single-Point Ablation

In this section we derive a methodology to learn the temporal evolution of tissue temperature during single-point laser ablation. Let $T(R, k) \in \mathbb{R}^{m \times n}$ be the two-dimensional matrix representing the temperature of R at the discrete time step k, assuming that $k = 0$ coincides with the time instant when the interaction starts. The temperature of any point $x, y \in R$ will be given by the (i, j)-element of the matrix, following the quantizations,

$$i = \left\lceil \frac{y}{\Delta_y} \right\rceil, \; j = \left\lceil \frac{x}{\Delta_x} \right\rceil \tag{4.8}$$

where $\Delta_y = Y/m$, $\Delta_x = X/n$, and the $\lceil \cdot \rceil$ notation expresses the ceil function, i.e., *the smallest integer not less than*.

Temperature of the surface is not uniform and changes with time, i.e.,

$$T(R, k) = f(x, y, k). \tag{4.9}$$

where $(x, y) \in R$ correspond to the pixel coordinates of any point on the surface. Based on the ideas presented in the previous section, we define a hypothesis function given by a Gaussian function with variable parameters,

$$T(R, k) = A(k) \exp\left(-\left(\frac{(x - \mu_x(k))^2}{2\sigma_x^2(k)} + \frac{(y - \mu_y(k))^2}{2\sigma_y^2(k)}\right)\right) \tag{4.10}$$

where A represents the amplitude σ_x and σ_y the spatial spreads of the Gaussian, and μ_x, μ_y the center of the function. Note that this hypothesis assumes symmetry with respect to the xy axis in the energy distribution delivered by the laser. Thus, this model can represent elliptical temperature profiles without rotation.

4.2.1 Fitting a Gaussian Function

A thermal camera is used to collect data for the learning task. At each time step, this provides a set of points $\left\{(x, y)^i, T^i\right\}_{i=1}^{m \times n}$ points from which the vector of parameters $\theta(k) = \left[A, \sigma_x^2, \sigma_y^2, \mu_x, \mu_y\right]$ needs to be estimated. A common approach is to use a linear version of the model, which is obtained by applying a logarithmic operator to both sides of the equation,

$$\log T = \alpha_0 + \alpha_1 x + \alpha_2 y + \alpha_3 x^2 + \alpha_4 y^2. \tag{4.11}$$

Hence, the nonlinear regression for (4.10) is transformed into a linear regression with *meta parameters*, $\alpha \in \mathbb{R}^5$ [4]. The elements of θ are then given by,

$$\begin{aligned} \sigma_x^2 &= -(2\alpha_4)^{-1} && , \sigma_y^2 = -(2\alpha_3)^{-1} \\ \mu_x &= \alpha_2 \sigma_x^2 && , \mu_y = \alpha_1 \sigma_y^2 \\ A &= \exp\left(\alpha_0 + \tfrac{\mu_x^2}{2\sigma_x^2} + \tfrac{\mu_y^2}{2\sigma_y^2}\right). \end{aligned} \tag{4.12}$$

A least square regression can then be applied to fit the sensor data in (4.11). Nevertheless, given that there is more data in the tail of the Gaussian than in the bell, weighting the sample points by its correspondent estimation balance the influence of the entire data set during the minimization of the sum of square errors. This is known as weighted least-square minimization (see [5]).

4.2.2 Meta-Parameters Dynamics

Fitting the hypothesis function (4.10) to the data captured during a real laser exposure provides a different vector of parameters for each time step. Figure 4.2 shows data corresponding to different times during laser exposure. In order to estimate the temperature at any point and time using such model a lookup table of hundreds of vectors of parameters would be required.

We propose to investigate a function describing the dynamics of the parameters $\theta(k)$, i.e. given the initial value $\theta(0)$ and an input $u(k)$ signal, the evolution of such parameters can be described using,

$$\theta_i(k+1) = h(\theta_i(k), \theta_i(0), u(k)), \tag{4.13}$$

where $u(k)$ may assume one of the following values:

$$u(k) = \begin{cases} 1 \ \textit{laser on/heating} \\ 0 \ \textit{laser off/cooling} \end{cases} \tag{4.14}$$

At the same time, it is important to note that the sequence of Gaussian parameters include errors from the noise in the raw data. Furthermore, these errors are propagated by the use of the logarithmic linear regression method and by the mapping from the meta parameters in (4.12). This is especially true for the amplitude (A), which is derived from a nonlinear function of the entire vector of meta parameters. To prevent the propagation of noise from further affecting the quality of the estimation (i.e., the quality of h) we propose to model the evolution of the meta parameters, i.e.,

$$\alpha(k+1) = g(\alpha(k), \alpha(0), u(k)). \tag{4.15}$$

The quality of g in (4.15) is expected to be better than the one of h in (4.13), given the level of noise in the respective data set.

4.2.3 Experiments

This section describes the experiments performed to capture the data to learn and validate the model. Single spot laser radiations on agar-based phantom tissue were produced using a CO_2 laser system. Temperature of the surface is captured continuously during laser exposure plus a proportional time after the laser is turning off in order to capture the cooling down process. Exposure time was precisely controlled with a computerized system.

Experiment Procedure

Each experiment consisted in firing a CO_2 Continuous Wave (CW) beam at constant power (P = 3W) on the flat surface of a tissue phantom. A different agar sample was used for each experiment. Samples were stored in a refrigerated bath and taken out at room temperature (∼25 °C) 10 min before the experiment. The exposure time of each experiment was electronically controlled and an independent sequence of thermal images was recorded. A total of 26 experiments were conducted, varying the exposure time from $t_{exp} = 2.0$ s to $t_{exp} = 4.5$ s with increments of 0.1s.

Data Sets

To solve the approximation problems formulated in Sects. 4.2.1 and 4.2.2 different data sets were created. Here we describe the structure and the content of these sets.

The former is a fitting problem, it aims to find the optimal Gaussian parameters θ_k that represent the superficial temperature at any time step k. This problem was applied to all of the thermal video frames captured during the laser experiments. During each experiment, a total of $(t_{exp} + t_{off}) \times 100$ frames were captured, each being a matrix with $l = m \times n = 3402$ values of temperature. Frames taken both during the laser exposure and the cooling off phase were considered.

Every experiment corresponds to a sequence of fitted Gaussian parameters θ_k, each representing the time evolution of temperature. These sequences are used to generate the input ($\mathbf{x}$) and output ($\mathbf{y}$) vectors required to learn function described in Eq. 4.13:

$$\mathbf{x} = [\theta_k^i, u_k^i] \tag{4.16}$$

$$\mathbf{y} = [\theta_{k+1}^i]. \tag{4.17}$$

Note that the input incorporates the laser input term u_k^i, which is required to estimate the variation of the values of parameters.

4.2.4 Results

Here we present the results for the Gaussians fitting of the single thermal images, the models obtained after learning the meta parameter dynamics and the temperature prediction that resulted from this data.

Gaussian Fitting

As mentioned in the previous section, a total of $(t_{exp} + t_{off}) \times 100$ Gaussians are approximated. Figure 4.3 shows an example data set and the corresponding

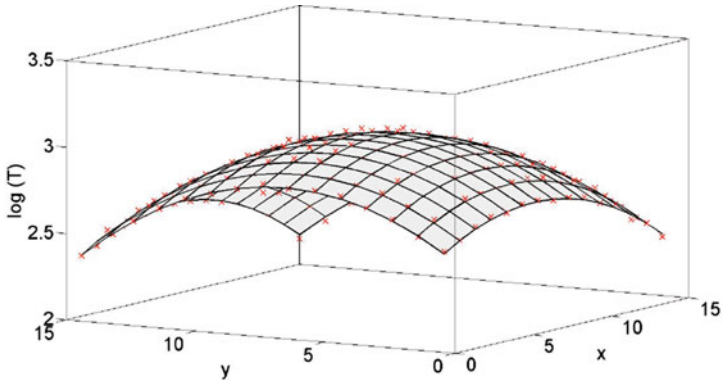

Fig. 4.3 The surface represents the linear regression obtained for input space (x, y) mapping to $z = \log(T)$, using the sensor data (*red* markers). Note that this is not the geometrical representation of the tissue. Reproduced from [3] with kind permission from Springer Science+Business Media

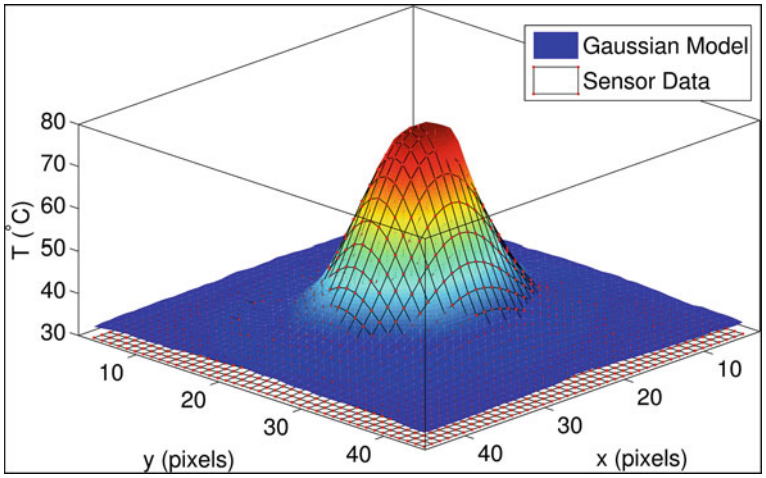

Fig. 4.4 Weighted least *square* estimation of the Gaussian model for a single time step. Corresponding parameters are $\mu = [9.27 \;\; 7.67]$, $\sigma^2 = [26.5 \;\; 15.78]$ and $A = 60.6457$, Approximation error (mse) = 0.0156. Reproduced from [3] with kind permission from Springer Science+Business Media

logarithmic linear regression. Figure 4.4 shows the result of fitting the thermal imaging sensor data to the hypothesis function in Eq. (4.10). The approximation error varies depending on the time of exposure. The temporal evolution of the normalized and root mean squared errors are presented in Fig. 4.6. It can be observed that the approximation of most of the frames present relatively low errors. Nonetheless, for the initial frames the approximation has high values of normalized mean square error (nMSE), indicating that the assumption of Gaussian shape is not completely verified. On the other hand, these frames present only a few Celsius of absolute average error

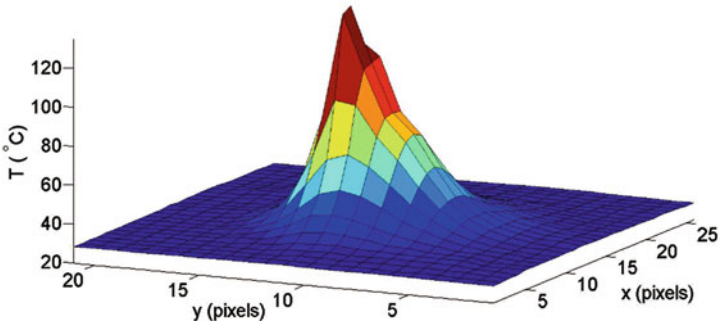

Fig. 4.5 Initial frames include high peaks of temperature that are not modeled by the Gaussian function. The peak points correspond to ablated tissue. Reproduced from [3] with kind permission from Springer Science+Business Media

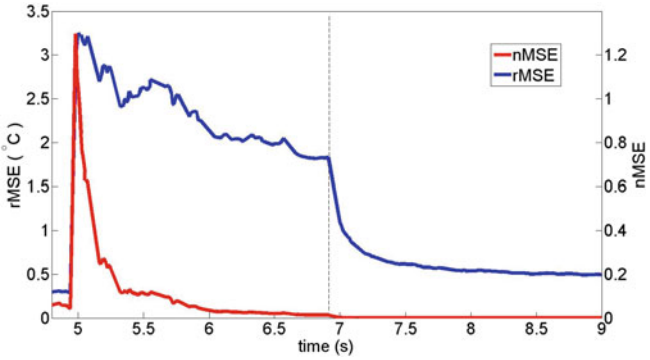

Fig. 4.6 Gaussian function approximation error for a complete experiment. RMSE (*blue*) and nMSE (*red*) changes depending on the stage of the interaction. The nMSE tends to zero after the initial time steps. Reproduced from [3] with kind permission from Springer Science+Business Media

(RMSE). Visual analysis of the initial frames reveals that these errors are largely due to the presence of the temperature peaks at the center of the beam (Fig. 4.5). These peaks are values of temperature at the center of the beam that last only one time step ($\Delta t = 0.01$ s) and we consider as noise. As we have commented earlier in this chapter, these peaks might have the following physical explanation, i.e. that they correspond to the expulsion of material from the ablation site—for which, therefore, temperature monitoring is not relevant.

Temporal Evolution of the Gaussian Parameters

Figure 4.7 shows the temporal evolution of the Gaussian parameters A, σ_x^2, σ_y^2 during a total exposure time and laser power similar to those used in laryngeal surgery

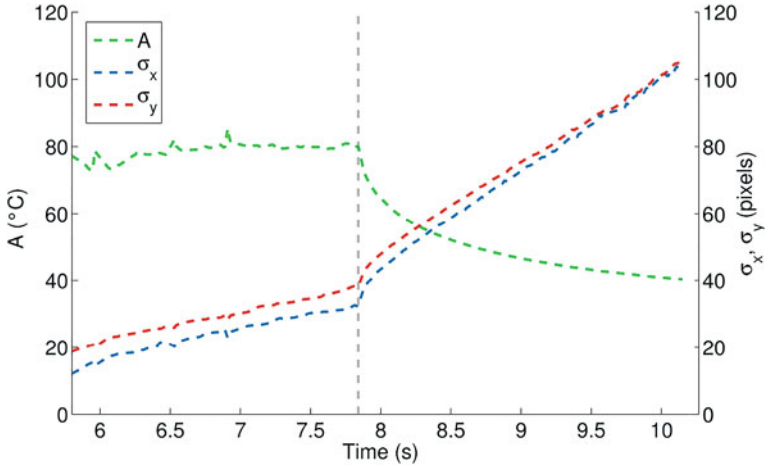

Fig. 4.7 Time evolution of the Gaussian parameters (A, σ_x, σ_y) during a $t_{exp} = 2\,\text{s}$ interaction ($t_0 = 5.8\,\text{s}$, $t_f = 7.8\,\text{s}$). It includes the heating and cooling phases. Reproduced from [3] with kind permission from Springer Science+Business Media

($P = 3.0$ W, $t_{exp} = 2\,\text{s}$). As expected, the parameters evolve differently when the laser is turned on. Different versions of Eq. (4.13) need to be learned to model both behaviors (heating, cooling) although the underlying structure of the hypothesis remains the same.

During laser exposure the amplitude of the Gaussian remains rather constant (Fig. 4.7), while the spread of the temperature over the tissue clearly increases. The instantaneous peaks of temperature observed in the center of the beam are naturally filtered by the linear regression.

When the laser is turned off the maximum temperature decreases and the rate of change of the variance increases. This is consistent with the analytic solution of the (homogeneous) heat transfer equation, where the amplitude of the function is inversely proportional to the square root of time, while the variance is proportional to it [2]. It can also be observed that the behavior of σ_x^2 and σ_y^2 are similar but not exactly the same: although the energy density produced by our laser is cylindrically symmetric (TEM_{00}), the orientation of the camera with respect to the target introduces a perspective deformation. This deformation was kept under control maintaining the position of the camera constant throughout the experiments. The sequence of means (μ_x, μ_y) is not showed as it remain almost constant throughout the experiment.

Dynamics of the Metaparameters

The exponential time evolution shown by the meta parameters in Fig. 4.8 suggests a first order dynamics for g of the form,

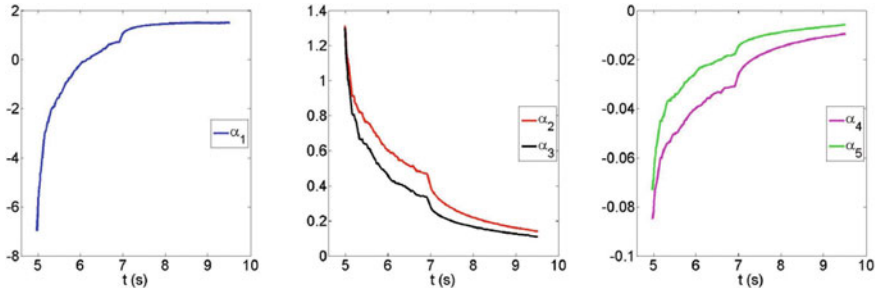

Fig. 4.8 Meta parameters time evolution α_1 (*blue*), α_2 (*red*), α_3 (*black*), α_4 (*green*), α_5 (*magenta*). Reproduced from [3] with kind permission from Springer Science+Business Media

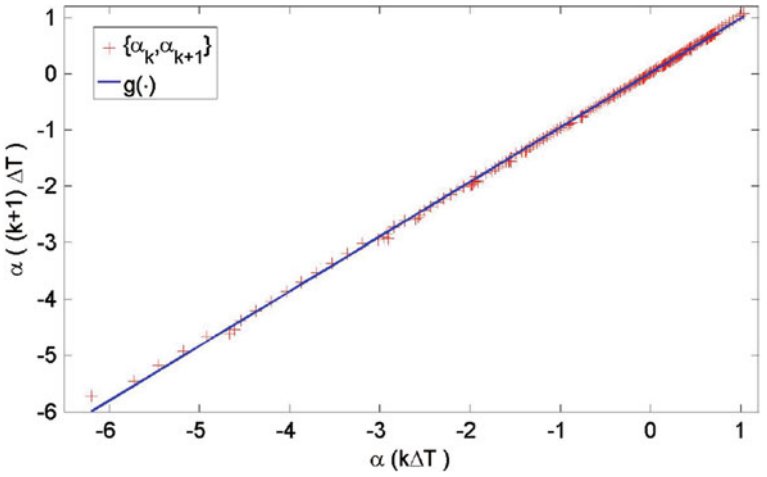

Fig. 4.9 First order dynamics in the meta parameter space $\alpha(k)$, $\alpha(k+1)$. Reproduced from [3] with kind permission from Springer Science+Business Media

$$\begin{aligned} \alpha(k+1) &= g(\alpha(k), \alpha(0)) \\ \alpha(k+1) &= C_1\alpha(k) + C_0 \end{aligned} \tag{4.18}$$

where C_1 and C_0 can be extracted with a simple polynomial regression between $\alpha(k+1)$ and $\alpha(k)$, as shown in Fig. 4.9. Simplified plots of the discrete dynamics of the meta parameters (both for heating and cooling models) are shown for completeness in Fig. 4.10. The resulting model parameters (C_0, C_1) are presented in Table 4.1.

Temperature Estimation

The estimation of temperature only requires the initial state of the meta parameters vector, then the recursion in (4.18) evolves with the activation/deactivation of the

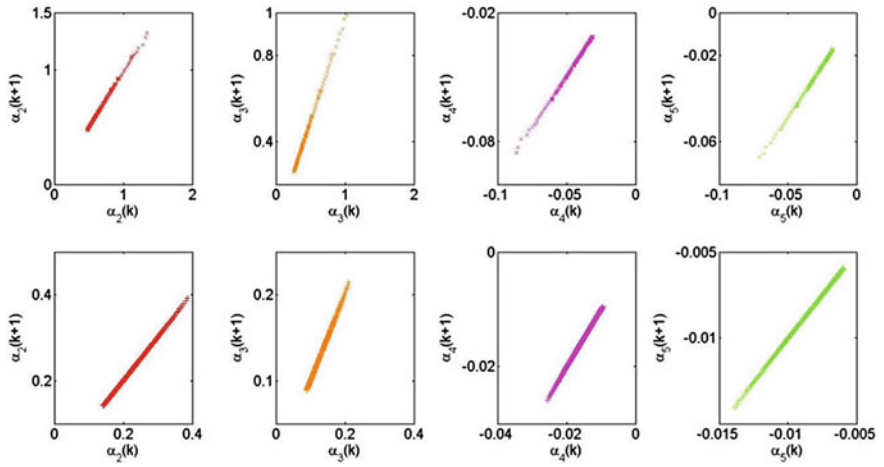

Fig. 4.10 Discrete dynamics of the meta parameters ($\alpha_i \quad i = 1, 2, 3, 4$). Both models are shown; 'laser on/heating' (*first row*) and 'laser off/cooling' (*second row*). Reproduced from [3] with kind permission from Springer Science+Business Media

Table 4.1 Table of constants for the meta parameters linear dynamics for both models: heating (laser on) and cooling (laser off)

α	$C0_{on}$	$C1_{on}$	$C0_{off}$	$C1_{off}$
1	0.9637	0.0333	0.9557	0.0772
2	0.9705	0.0155	0.9869	0.0019
3	0.9646	0.0108	0.9864	0.0012
4	0.9716	–0.0010	0.9876	–0.0001
5	0.9649	–0.0007	0.9879	–0.0001

Reproduced from [3] with kind permission from Springer Science+Business Media

laser input. The Gaussian parameters and therefore the surface temperature can be estimated at any time of interest. Figure 4.11 shows the comparison between the real time change of the meta parameters and that obtained with the recursion. Figure 4.12 shows an example of surface temperature reconstruction (nMSE = 0.0137).

4.2.5 Discussion

The model presented in this section is able to predict temperature of the surface of tissue gel phantoms during single point CO_2 laser ablation. The modeling process takes advantage of the Gaussian structure of the data and here we explain such structure analyzing the shape of the energy spatial profile in the laser beam.

Although the hypothesis function allows us to model elliptical shapes for the Gaussian, it assumes that it is not rotated. Due to the physical location of the sensor

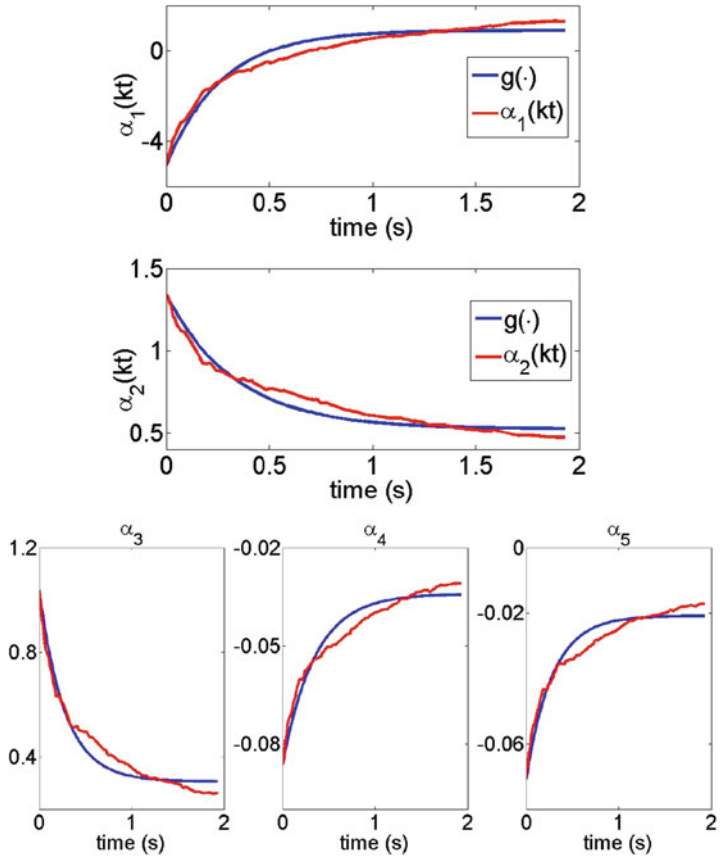

Fig. 4.11 Time evolution of the meta parameters (α_i). Learned dynamics (*blue*) extracted from data (*red*). Reproduced from [3] with kind permission from Springer Science+Business Media

some perspective was generated and data captured by the thermal camera showed that minor rotation were present. The model can be augmented, including parameters for the xy distribution of temperature, improving the fitting error. This fitting error may also be improved using an iterative method for Gaussian approximation [5].

The assumption that the dynamics of the meta parameters α is easier to model than the one of the Gaussian parameters θ can be observed in Fig. 4.13, where the sequence of values for the first element of both sets is shown. It can be seen that the pattern of α_1 can be described using a first order dynamics, whereas that of θ_1 is much more complicated to describe.

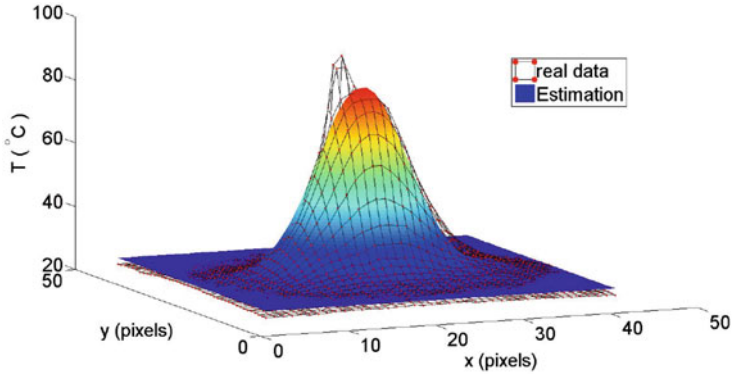

Fig. 4.12 Temperature reconstruction. At a given time during laser exposure (t_{exp} = 1.92) the temperature of the surface is estimated using the evolution of the meta parameters with nMSE = 0.0137. Reproduced from [3] with kind permission from Springer Science+Business Media

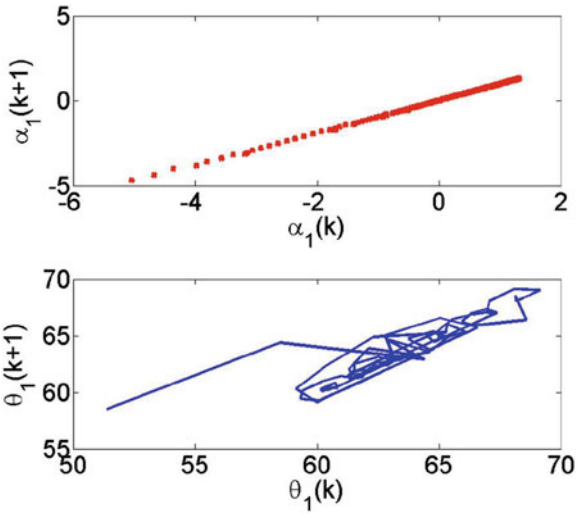

Fig. 4.13 Discrete dynamics of the first element of the meta parameter vector (α_1) as well as of the Gaussian parameter (θ_1). The pattern of $\alpha_1(k)$ can be modeled with a first order system. Reproduced from [3] with kind permission from Springer Science+Business Media

4.3 Temperature Dynamics During Laser Scanning

We now seek to extend our modeling methodology to the more general case of tissue ablation by means of a scanning laser beam. The motion of the laser beam directly affects the time-dependent energy density S, thus determining a different thermal response. Evidence presented so far in this chapter indicates that, in the case of single point ablation, the temperature $T(t)$ on the surface of tissue may be modeled by a single Gaussian function with time-varying parameters. The use of a moving laser beam imposes the use of a different model, whose structure is determined experimentally, from the analysis of data collected during preliminary laser trials.

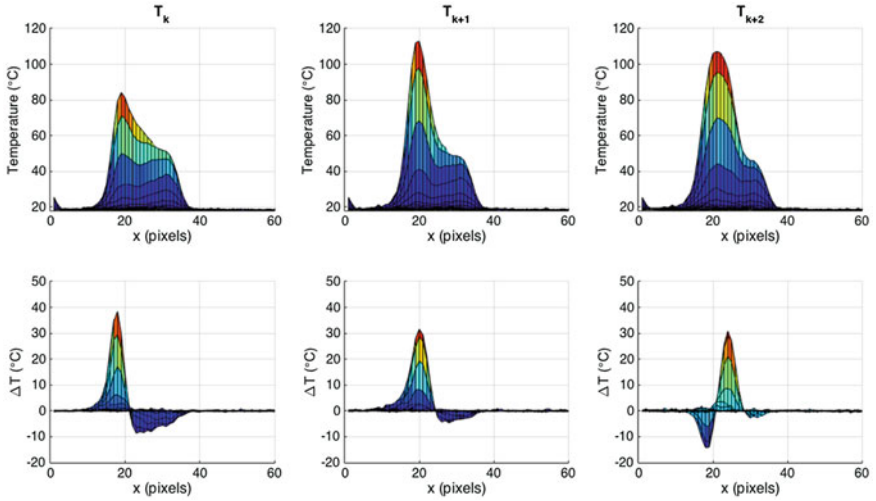

Fig. 4.14 *First row* Tissue temperature profile during computer controlled incision ($l = 0.3$ mm, $w = 10$ Hz). Although the Gaussian distribution of the energy in the laser beam is present, the profile does not show any particular pattern as it grows in time. *Second row* Temporal change on temperature $\Delta T = T(R, k+1) - T(R, k-1)$. Adapted from [6]

Incisions were created on ex-vivo chicken muscle tissue samples, by means of a laser scanning system (described in Sect. 3.6.1). The laser beam is moved repeatedly along a line of length ($l = 4.6$ mm), during certain exposure time (t_{exp}). The motion of the laser scans the complete line at a configurable velocity and oscillatory frequency (ω_s). Therefore, the number of times the laser scans the incision is given by $\eta = t_{exp}/\omega_s$. The period of time the tissue is exposed to the laser is uniformly distributed along the incision line.

Examples of the superficial temperature profile for different times k of the process $T(R, k)$ are shown in the first row of Fig. 4.14. With the aim of reducing the problem complexity, we take the y axis to be coincident with the laser scanning trajectory. We further assume symmetry with respect to the incision line, thus only the temperature along the x axis is shown. The Gaussian-shaped contribution of the laser input S can be visually recognized in the correspondence of the temperature peaks. Nonetheless, as the beam moves along the incision, the temperature profile does not seem to present any specific pattern as it evolves in time.

The second row of Fig. 4.14 shows the temperature increments for the corresponding exposure time. These sequence suggests that the temporal increment of the temperature $\Delta T(k) = T(R, k+1) - T(R, k)$ could be described as a set of Gaussian functions with centers along the incision line. The positive part of ΔT seems always amenable to be described by a single Gaussian, while the negative part shows diverse conformations. Based on the heat conduction equation (2.12), the positive corresponds to the thermal effects of the input S plus the heat exchange with underlying and surrounding tissue. Thus, the center of this Gaussian is expected

to move together with the laser beam along the incision. The negative part of ΔT constitutes the effects of heat diffusion within tissue, which is modeled by the homogeneous part of the heat conduction equation (Eq. 4.5) by a second-order differential term. This indicates that the shape of the negative part should contain higher order differences of $T(R, k)$.

Based on these observations, we theorize that the function describing the temperature of the surface at each frame of the process can be approximated as a sum of Gaussian functions,

$$T(R, k) = \sum_{i=1}^{p} \exp(x, y, a_i, \sigma_i, \mu_i) \tag{4.19}$$

where p is the total number of Gaussians and a_i, μ_i and σ_i are the corresponding amplitude, mean and covariance. Nonlinear least square fitting regression [1] can be applied to fit (4.19) to the experimental data.

4.3.1 Experiments

Ex-vivo chicken muscle tissue is used as target for the incision trials. Incision length ($l = 4.6\,\text{mm}/25$ pixels) and scanning frequency ($\text{w} = 10\,\text{Hz}$) are kept constant. Laser power ($P = 3$ W), and exposure mode (Continuous Wave) were also configured. Total exposure time is set to $t_{exp} = 1.0\,\text{s}$.

4.3.2 Results

The x-axis is aligned with the incision line and the spatial distribution of the temperature is assumed to be symmetric with respect to the y-axis. Here we compare the quality of the model for different values of p. Based on the knowledge provided by (Eq. 2.12), we may hypothesize that the number of Gaussians required for the model is $p = 4$. Nevertheless here we compare the models for different values of p.

For the simplified case of one-dimensional distribution of temperature, the temperature on the incision line $T_k(x)$ is defined by the function

$$T_k(x) \approx \sum_{i=1}^{p} \exp(x, \mu_i, \sigma_i) \tag{4.20}$$

Each experiment is composed by 100 data sets ($t_{exp} = 1.0\,\text{s}$, $\Delta t = 0.01\,\text{s}$). The number of input-output pairs per data set is given by the width (in pixels) of the area of interest. Thus, the model is composed by a total of 100 regressions, each one is obtained using $m = 60$ data pairs $\{x_j, T_j\}_{j=1}^{m}$. Figure 4.16 shows three examples of function approximated.

Table 4.2 Regression results analysis: Mean square error (MSE) for $n = 100$ regressions

p	MSE_{max}	MSE_{min}	Mean	Median	Q3–Q1
3	17.57	0.24	3.42	2.93	2.03
4	6.87	0.21	2.31	1.99	1.72
5	4.67	0.23	1.85	1.63	1.35

Adapted from [6]

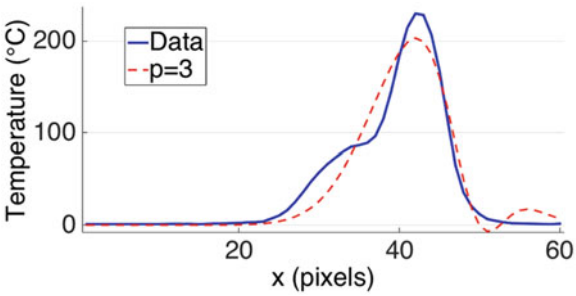

Fig. 4.15 Regression result ($p = 3$). Real temperature is also shown. Adapted from [6]

Modeling Error

The output of the regression at each time step is a vector of parameters (amplitudes, means and standard deviation), $\theta_k = [a_k, \mu_k, \sigma_k]$, where $a, \mu, \sigma \in \mathbb{R}^p$. Each data set generates an approximation error, i.e., it is variable along the experiment. The mean square error (MSE) is analyzed to compare the quality of the model for different values of $p = 3, 4, 5$. Table 4.2 summarizes the information about the variability of the regression error along the experiment, including maximum, minimum, mean, median and interquartile range. It can be seen that the model fits better when using more Gaussians: $p = 4$ performs better than $p = 3$, while not significant improvements can be observed by increasing the number of basis functions to $p = 5$. With $p = 4$, the regression achieves an accuracy (Root-Mean-Square Error) of 1.52 °C, with the largest error ($RMSE_{max}$) being 2.62 °C. Figure 4.15 shows the temperature estimation when modeling with few Gaussian basis functions. On the other hand, Fig. 4.16 shows three examples of regressions with $p = 4$. Different forms of temperature profile are shown.

4.3.3 Model Validation

Based on the analysis presented above, a model using $p = 4$ is selected to estimate the temperature dynamics during laser exposure. A total of 12 parameters for each time step are used for prediction.

In order to validate the model, a new experiment is performed and thermal data is captured while the model estimates the temperature profile. Validation error is

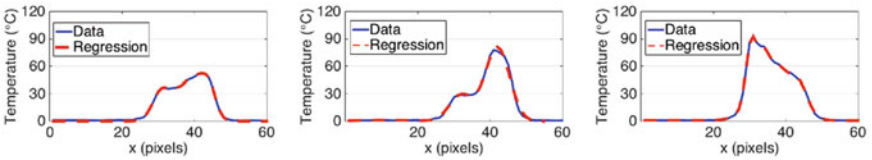

Fig. 4.16 Temperature profile at different stages of the incision. Continuous line (*solid blue line*) shows data collected from experiments, dash line (*red*) shows the result of the regression $p = 4$. Adapted from [6]

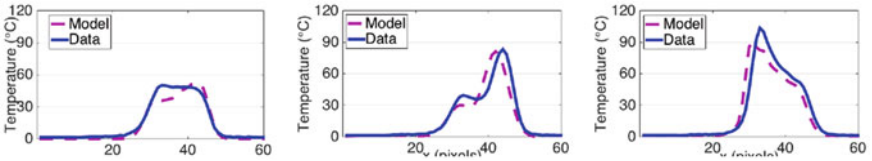

Fig. 4.17 Validation experiments. Sensor data (*solid blue line*) and the corresponding temperature predicted by the model (*dashed violet line*). Adapted from [6]

Table 4.3 Validation results analysis: Mean square error (MSE) for $p = 4$ and $n = 100$ regressions

MSE_{max}	MSE_{min}	Mean	Median	Q3–Q1
19.27	4.44	12.52	13.41	10.34

Adapted from [6]

computed pixel-wise during $t_{exp} = 1$ s. Figure 4.17 shows the real temperature profile for the validation experiment and the resulted temperature estimation (for the same time steps used in Fig. 4.16). It can be observed that the new experiment slightly varies with respect to the learning data set. This causes a relatively high pixel-wise error, as presented in Table 4.3.

Nevertheless, the range and distribution of the temperature is effectively estimated at each time step. In order to illustrate this, a comparison between the maximum value at each time step is shown in Fig. 4.18. It can be observed that the model captures the dynamics of the temperature change. The shape of the temperature profile is compared by computing the area under the curve at each time step, also shown in Fig. 4.18. It can be observed that the model is able to effectively estimate the thermal state of the tissue surface.

4.3.4 Discussion

The experimental evidence presented in this section indicates that statistical learning enables the creation of models capable of reliably estimating tissue temperature

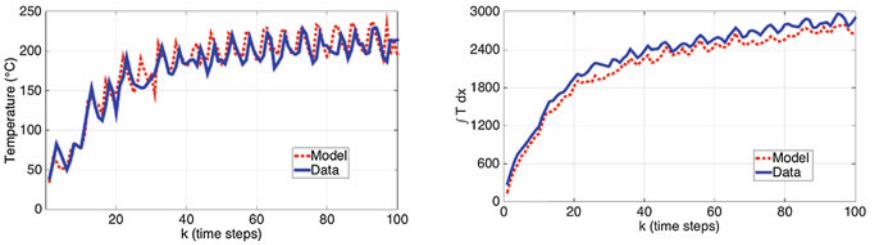

Fig. 4.18 Validation experiment. Maximum values of temperature for each time step are presented (*top*). The integral of the area under the curve for each time step is also presented (*bottom*). Adapted from [6]

variations during laser incisions. These models are straightforward to implement in a surgical setup, as they do not require any additional sensing device.

The model presented here was derived on ex-vivo chicken muscle tissue. Although not representative of the variety of tissues that are encountered during a laryngeal intervention [7], these targets present the behavior of a generic soft tissue, allowing to prove the proposed concept. Our modeling study does not explicitly take into account heat transfer mechanisms typical of living tissues, e.g. blood perfusion. Nonetheless, the contribution of these mechanisms to the local variation of temperature is neglectable in first approximation [2].

In Chap. 6, we shall describe the integration of this model in an experimental surgical platform. Activation and deactivation of the model will be synchronized with the laser activation, allowing online estimation of the temperature of the tissue surface.

References

1. D. Bates, D. Watts, in *Nonlinear Regression Analysis and Its Applications*, ser. Wiley Series in Probability and Statistics (Wiley, 2007)
2. M. Niemz, *Laser-tissue Interactions* (Springer, Berlin, 2004)

3. D. Pardo, L. Fichera, D. Caldwell, L. Mattos, Learning temperature dynamics on agar-based phantom tissue surface during single point co_2 laser exposure. Neural Process. Lett. **42**(1), 55–70 (2015). http://dx.doi.org/10.1007/s11063-014-9389-y
4. R.A. Caruana, R.B. Searle, T. Heller, S.I. Shupack, Fast algorithm for the resolution of spectra. Anal. Chem. **58**(6), 1162–1167 (1986)
5. H. Guo, A simple algorithm for fitting a gaussian function. IEEE Sig. Process. Mag. **28**(5), 134–137 (2011)
6. D. Pardo, L. Fichera, D. Caldwell, L. Mattos, in *Thermal Supervision During Robotic Laser Microsurgery*. 2014 5th IEEE RAS EMBS International Conference on Biomedical Robotics and Biomechatronics (2014), pp. 363–368
7. S.L. Jacques, Optical properties of biological tissues: a review. Phys. Med. Biol. **58**(11), R37 (2013)